RESEARCH ARTICLE

Key Points:
- Wind stress curl structures in EBUS
- SST-induced wind perturbations
- Orographic effects on winds

Correspondence to:
F. Desbiolles,
fabien.desbiolles@univ-brest.fr

Origin of fine-scale wind stress curl structures in the Benguela and Canary upwelling systems

F. Desbiolles[1,2], B. Blanke[1], A. Bentamy[2], and N. Grima[1]

[1]Laboratoire de Physique des Océans, UMR 6523 CNRS-Ifremer-IRD-UBO, Brest, France, [2]Laboratoire d'Océanographie Spatiale, Centre de Brest, Ifremer, Brest, France

Abstract Numerous studies have shown the primary importance of wind stress curl in coastal upwelling dynamics. The main goal of this new analysis is to describe the QuikSCAT surface wind stress curl at various scales in the Benguela and Canary upwelling systems. The dominant spatial pattern is characterized by cyclonic curl near continental boundaries and anticyclonic curl offshore, in association with equatorward alongshore (upwelling favorable) wind stress. At a smaller scale, we demonstrate the sensitivity of the QuikSCAT wind stress curl to coastal processes related to sea surface temperature (SST) mesoscale fluctuations by presenting a linear relationship between the curl and crosswind SST gradients. Despite the spatial and temporal sensitivity of the underlying thermal coupling coefficient, a local analysis of the fraction of the curl ascribed to SST variability shows that SST is a main driver of the wind stress curl variability and magnitude over the upwelling extension zone (~100–300 km from the coast) in both the Canary and Benguela systems. Closer to the shore, the curl patterns derived from QuikSCAT observations are only loosely related to SST-wind interactions. As a working hypothesis, they can also be associated with the coastline geometry and orographic effects that are likely to play an important role in local cooling processes.

1. Introduction

The ocean and atmosphere form a complex system in which many interactions and coupling processes coexist over a large spectrum of time and space variability. At the synoptic and global scales, it has generally been assumed that the atmosphere forces the ocean through energy inputs by the winds and by the radiative and turbulent (i.e., latent and sensible) heat fluxes. Specifically, the upper ocean circulation is mainly forced by the curl of the wind stress [*Gill*, 1982]. In the eastern boundary upwelling systems (EBUS), vertical mixing, geostrophic adjustments, and oceanic heat balance can be related to the spatial and temporal variability of the surface momentum fluxes [*Renault et al.*, 2009, 2012; *Colas et al.*, 2012]. Indeed, the wind stress (wind stress curl) plays a dominant role in determining the Ekman transport and coastal upwelling (near-shore Ekman pumping), and thus in forcing the sea surface temperature distribution and shaping the full three-dimensional ocean circulation over the continental shelf [*Fennel et al.*, 2012].

In contrast, on smaller spatial scales between 100 and 1000 km, the ocean affects the atmosphere, controlling surface winds through thermodynamical and dynamical, local and remote feedbacks [*Chang and Philander*, 1994]. For instance, wind speed and sea surface temperature (SST) perturbations show strong positive correlation in regions of significant midlatitude SST fronts, i.e., near meandering ocean currents [*Small et al.*, 2008; *O'Neill et al.*, 2010]. The main process that is involved here is an interaction between SST and the height of the marine atmospheric boundary layer (MABL). More precisely, the cooling of air above cold water increases the stratification of the lower atmosphere, stabilizes the MABL, and thus decreases both vertical turbulent mixing and convection [*Song et al.*, 2009]. This process uncouples the surface winds from the more intense flow at elevations above the top of the planetary boundary layer and increases the vertical wind shear near the sea surface. Some of these thermal coupling processes were sketched by *Businger and Shaw* [1984] (see schematic diagram in their Figure 10) and since then the surface implications, i.e., the deceleration (acceleration) of the wind over cold (warm) waters satisfying a roughly linear relationship, have been quantified over mesoscale coherent structures [*Chelton et al.*, 2004; *O'Neill et al.*, 2005; *Small et al.*, 2008].

The SST distribution in EBUS reflects both the Ekman-induced cross-shore temperature gradient and the mesoscale characteristics of the upwelling dynamics, notably with the presence of numerous eddies and meanders. *Chelton et al.* [2007] and *Haack et al.* [2008] have demonstrated that a significant SST-wind

feedback is expected over such structures in the California upwelling system, with SST being able to modify the winds. The parameterization of this feedback in an ocean model can help reduce the biases associated with the inshore extrapolation of satellite wind observations near the coast, via wind reduction over colder SST as shown by *Jin et al.* [2009] for the northeastern Pacific Ocean. This decrease in coastal wind intensity allows reduction of the intensity of the upwelling and of the cold bias usually modeled at the coast. The result is a modification of the coastal current system linked to the upwelling dynamics [*Marchesiello et al.*, 2003].

The dynamics of an upwelling zone responds to the spatial structures observed in the wind at fine scale and high frequency [*Carr*, 1998; *Pickett and Paduan*, 2003; *Blanke et al.*, 2005]. This atmospheric variability can, in turn, be altered by several physical processes in the nearshore region. In addition to coupling processes over SST fronts, orographic effects and perturbations induced by a rugged coastal area become progressively more important, complicating the structure of the wind stress curl [*Chelton et al.*, 2007]. This coastal transition zone may extend more than 100 km offshore [*Boé et al.*, 2011]. These sea-land processes and air-sea interactions often contribute to the weakening of the coastal winds and, thus, to the reduction of the coastal upwelling cooling and to the increase of local curl-driven Ekman pumping. According to *Marchesiello and Estrade* [2010], the space scale of the coastal upwelling response is generally finer than the scale of the wind dropoff, which leads to local imbalance between the vertical velocities generated either by the increase of Ekman pumping or the decrease of coastal upwelling. The direct measurement of realistic coastal wind profiles is still a difficult task, though airborne experimental studies have been implemented in EBUS and proved successful in describing the role of fine-scale wind patterns during a strong and persistent upwelling event [*Münchow*, 2000]. The orography-induced wind stress curl acts on the fine dynamics scales of the upwelling circulation as demonstrated by the high sensitivity of the nearshore ocean to the spatial organization of the wind stress curl [*Marchesiello et al.*, 2003; *Capet et al.*, 2004]. Orographic effects may also lead to wind intensification, which contributes to the local modification of the balance between Ekman transport and Ekman pumping [*Perlin et al.*, 2004].

During the last two decades, significant improvements in surface wind observations over the global ocean have been achieved, both for speed and direction. Measurements are mainly retrieved from scatterometers such as the European Remote Sensing Satellites (ERS1/2), Advanced Scatterometer (ASCAT), and Quick Scatterometer (QuikSCAT). Such remote sensing data have allowed a better description of the surface winds and, therefore, led to improvements in numerical ocean simulations (e.g., *Burls and Reason* [2008], in their modeling of the Southern Benguela upwelling system). It is worth noting that some studies advise against the use of older-generation satellite winds (with approximately half-degree horizontal resolution) to force oceanic numerical models [see, for example, *Renault et al.*, 2012]. Today, space missions involving new scatterometer instruments aim at improving the global fine spatial and temporal resolution of the wind stress (25 km daily, or even 12.5 km), knowing that temporal sampling of fast atmospheric variability and data contamination by the land-ocean transition and by rain remain issues of concern [*Bentamy and Croizé-Fillon*, 2011]. Improvements in the retrieval algorithms and new spatial grid resolutions lead to wind products that can be suitable for the study of wind-sea interactions in EBUS.

The main purpose of this study is to investigate and describe joint wind stress curl and SST patterns off the western coast of Africa, using satellite gridded data sets with a spatial resolution of $0.25°$ in longitude and latitude, i.e., the daily QuikSCAT zonal and meridional wind stress components distributed by CERSAT (Centre ERS d'Archivage et de Traitement) and the so-called Reynolds SST [*Reynolds et al.*, 2007]. After showing the imprint of ocean surface patterns on satellite winds over the Atlantic EBUS (section 3), we identify the locations where SST has the largest effect on the low-level wind, and we analyze the magnitude and variability of the SST-driven curl (section 4). Section 5 focuses on a comparison about sea-wind coupling between the new and the former generation of satellite wind stress. Our concluding remarks are presented in section 6.

2. Data and Methods

2.1. Data

For the past 20 years, outstanding efforts have been made to describe and understand the atmospheric conditions at the sea surface. An increasing number of space missions and major technical improvements

have allowed the refinement of the space and time resolution of the products available at global scale. Satellite scatterometers continuously provide valuable surface wind speed and direction observations over the global ocean. This study employs only wind retrievals from the SeaWinds scatterometer on board QuikSCAT. A complete description of this instrument can be found in *JPL* [2006], including instrument physics, retrieval and ambiguity removal methods, rain detection and flagging techniques, and quality control procedures.

Briefly, QuikSCAT is a Ku-band radar using a rotating antenna with two emitters with observation swaths of 1400 and 1800 km that cover around 90% of the global ocean daily. The ascending and descending scatterometer observations are both from the new QuikSCAT L2b products (known as JPLV3 products [*Fore et al.*, 2014]). The QuikSCAT wind retrievals are provided within the swath into 12.5 km wind vector cells. The new scatterometer product is assumed to improve the wind speed performance in rain and at high wind speed conditions. The retrievals are routinely used to estimate daily global wind fields with a spatial resolution of 0.25° in longitude and latitude (Level 3 product, hereafter QS25). All quality controls relying on quality flags associated with the L2b product (wind retrievals) are used for wind data selection. For instance, data relying on measurements plausibly contaminated by the antenna sidelob envelope are not selected. Level 2 data have been significantly improved in the coastal band with an approximate 12.5 km blind zone off the coast [*Stiles*, 2014]. Any L2 cell that includes parts of exploitable swaths for a given day is labeled as "ocean." Other grid cells are masked. The objective analysis, the processing for daily scatterometer analyses developed at Ifremer (Institut Français de Recherche et d'Exploitation de la Mer) and its accuracy are detailed by *Bentamy et al.* [2011, 2013]. For instance, the QS25 wind quality is investigated through comprehensive comparisons with daily buoy estimates. The accuracy results based on the collocated QS25 and National Data Buoy Center (NDBC) buoy moored in the California upwelling system within 50 km of the coast indicate that the wind speed is slightly overestimated by the scatterometer data (with a bias of about 0.60 m/s). However, the root mean square (rms) difference does not exceed 1.60 m/s, and the correlation coefficient is as high as 0.88. Although the zonal and meridional components show higher values of the rms difference (up to 2 m/s), mainly attributable to ambiguity removal issues, the correlation between QS25 and buoy daily components is high (0.90). The vector wind stress is calculated from the QS25 10 m neutral stability wind with the *Fairall et al.* [2011] bulk formulation. The wind data used in this study can be accessed freely (ftp://ftp.ifremer.fr/ifremer/cersat/products/gridded/MWF/L3/QuikSCAT/Daily/).

We also use the former QuikSCAT L3 product with 0.5° resolution in longitude and latitude (hereafter QS50) to investigate explicitly the improvements allowed by the finer spatial resolution of the surface wind on the study of SST-wind interactions. The temperature data set used in this study is the Reynolds SST [*Reynolds et al.*, 2007], which is a reconstruction by optimal interpolation of daily SST fields derived from two high-resolution satellite datasets: Advanced Very High Resolution Radiometer (AVHRR) and Advanced Microwave Scanning Radiometer (AMSR). In situ data from ships and buoys are also used in the analysis. One main advantage of the Reynolds SST is its full availability at the same resolution as QS25 (0.25° in longitude and latitude). The Reynolds SST can be freely downloaded (ftp://eclipse.ncdc.noaa.gov/pub/OI-daily-v2/NetCDF/).

Our joint analysis of SST and wind curl patterns is conducted over a full 5 year period, from 1 January 2004 to 31 December 2008. This sequence corresponds to the first 5 years available in full in the QS25 data set.

2.2. Methods

The atmospheric response to SST forcing has been investigated by numerous studies, but, to our knowledge, no results deal with the meandering SST fronts observed in both the Canary and Benguela upwelling systems. Building on the studies that highlighted the SST influence on the wind [e.g., *Chelton et al.*, 2004], one can decompose the total SST gradient vector into local crosswind and downwind components, $|\nabla SST \times \hat{k}| = |\nabla SST| \sin(\theta)$ and $\nabla SST \hat{k} = |\nabla SST| \cos(\theta)$, where $\hat{k}$ is the unit vector aligned with the direction of the wind stress and θ is the counterclockwise angle from the vector ∇SST to $\hat{k}$. We focus here on the spatial variability of the wind stress curl and on the related crosswind SST gradient. Both fields are first averaged in overlapping 7 day bins sampled at daily intervals. Indeed, as discussed previously, the first-order effect of the air-sea coupling in EBUS (for time scales from one to a few days) is a one-way forcing of the ocean by the atmosphere, which results in the structuring of a well-developed SST front. Here on a weekly time scale, one can hypothesize that the SST distribution also feeds back on the low-level wind field. This assumption is confirmed by the increase of the linear correlation coefficient between SST and wind stress time series from daily to weekly time scales. It is worth reminding here that a positive (negative) correlation between

Table 1. Mean Correlation Coefficient Between the Crosswind SST Gradient and QS25 Wind Stress Curl Over the Full Time Series (2004–2008) in the Southern Benguela Upwelling System[a]

Averaging window (in days)	1	3	5	7	10	15	20	25	30
Correlation coefficient	0.09	0.18	0.21	0.30	0.31	0.37	0.41	0.43	0.46

[a]The correlation is calculated for various sizes of the moving window used for time averaging both fields.

SST and wind stress usually indicates that SST (wind) exerts an influence on the surface wind (SST) [*Xie*, 2004]. Table 1 shows that the mean coefficient calculated over the Southern Benguela system starts from negligible values at daily scale, and becomes positive and important when the averaging period increases to 7 days. This is especially true over the upwelling extension zone (∼100 to 300 km off the coast; see section 3.3). The statistical significance of each regression was tested with a Monte Carlo technique, by comparing the squared correlation to that of a randomly scrambled ensemble. The values in Table 1 are averages and do not reflect some high correlation coefficients (greater than 0,6) found with a 7 day window at some locations.

3. Dynamical Background, Thermal Coupling Process, and Spatial and Temporal Sensitivity

3.1. Alongshore Wind Stress, Wind Stress Curl Structures, and Upwelling Variability

The synoptic scales of the atmosphere drive the upwelling dynamics at the western African coast through the trade winds. They wrap around large-scale atmospheric systems and flow toward the intertropical convergence zone. The resulting alongshore wind stress controls the divergence of the seaward Ekman current and causes cooling in the upper ocean in both the Canary and Benguela upwelling systems. The seasonal shift of the large-scale atmospheric anticyclones translates into modulations of the coastal upwelling through seasonality of the trade winds [*Wooster et al.*, 1976]. The austral (boreal) summer is the preferred upwelling season in the Southern Benguela (Northern Canary) system. In both regions, basin-scale wind patterns contribute to the layout of the wind stress curl, with a coastal band of important cyclonic (upwelling favorable) values and weak anticyclonic values offshore (Figure 1). The topographical forcing induced by capes and inhomogeneities of the coastline favors the strengthening of the wind stress curl near the coast. This is especially the case downwind Cape Blanc (21°N) for the Northern Hemisphere (see Figure 1c), and downwind Cape Columbine (33°S) for the Southern Hemisphere [*Desbiolles et al.*, 2014] (see Figure 1a). Local phenomena such as orographic effects and thermal coupling can also shape the coastal wind stress curl.

Following the description of seasonal upwelling dynamics in the Benguela and Canary systems (see *Duncombe Rae* [2005] and *Lathuilière et al.* [2008], respectively), both areas can be split into two subregions, with contrasted space-time patterns of the alongshore wind stress component. The separation latitude of the Benguela upwelling subsystems is usually taken at 26.5°S, i.e., the approximate latitude of the permanent Lüderitz cell. Further north, upwelling-favorable winds blow all-year long. The Southern Benguela system (from 34°S to 26.5°S) is characterized by strong seasonality in Ekman transport with an intense coastal upwelling during austral summer, i.e., from December to February [see *Desbiolles et al.*, 2014, Figure 12a]. The Canary upwelling system is usually split between 20°N and 22°N and shows strong contrasts in upwelling-favorable wind seasonality, in line with the meridional shift of the trade winds. South of 22°N, the Ekman transport climatology shows pronounced variability with a period of intense upwelling from November to July and relaxation around September. The border zone between both subregions (20°N–22°N) is characterized by permanent, strong upwelling-favorable winds and, thus, sustained offshore Ekman transport throughout the calendar year. The northern subregion is associated with weaker seasonal variability than its southern counterpart. The wind blows equatorward all year long, although with reduced intensity in winter [*Troupin et al.*, 2012] because of the northward migration of the Azores High [*Wooster et al.*, 1976]. Therefore, upwelling dynamics is active throughout the year, but is more intense during summer [see *Desbiolles et al.*, 2014, Figure 9a]. In the Cape Ghir region, the wind intensity is increased both in summer and winter, probably under the influence of the High Atlas, a mountain range in Morocco oriented west to east (see Figure 6). The complex oceanic dynamics is forced by the wind stress and the orography-induced wind stress curl, and gives rise to the recurrent Cape Ghir filament [*Troupin et al.*, 2012].
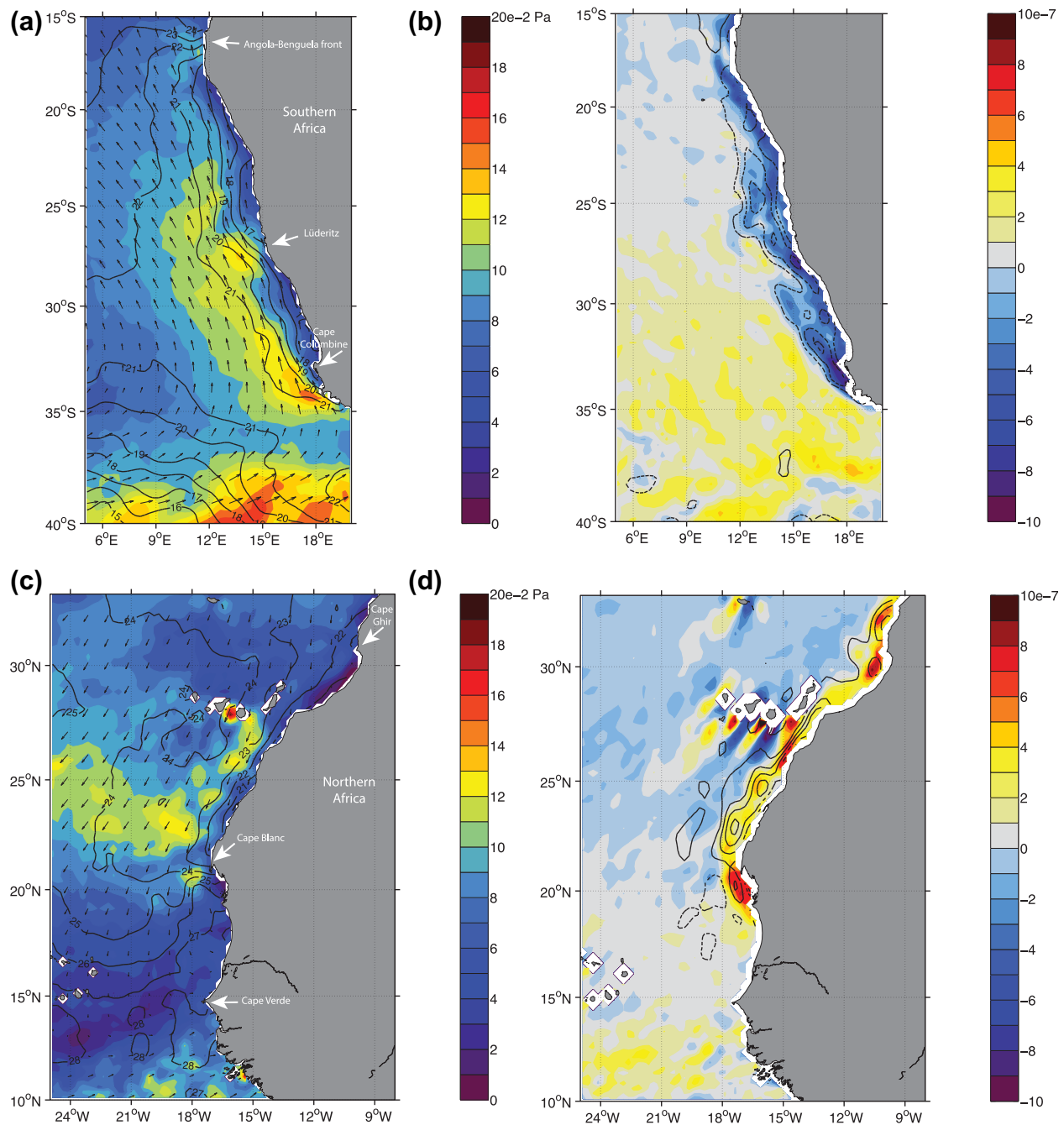
Figure 1. (left) Wind stress intensity (color, in Pa) and vectors (black arrows), and SST (black contours, with a 1°C interval) averaged (a) over December 2004 to February 2005 in the Benguela upwelling system and (c) over July 2005 to August 2005 in the Canary upwelling system. (right) Wind stress curl (color, in Pa/m) and crosswind SST gradient (contours, with a 5·× 10^{-5}°C/m interval and dashed negative values) over the same periods in the (b) Benguela and (d) Canary upwelling systems.

3.2. SST Feedback

Summertime, i.e., December-February and June-August for the Benguela and Canary systems, respectively, is the dominant season for upwelling-favorable winds along the coast. More precisely, summertime is the only season when steady trade winds blow equatorward, parallel to the coast, in the Southern Benguela and the Northern Canary regions. This atmospheric regime results in the resurgence of cold water in the coastal fringe (Figures 1a and 1c, for the Benguela and Canary systems, respectively). When the surface wind blows steadily along an SST front, the wind is decelerated on its cold side and accelerated on its warm
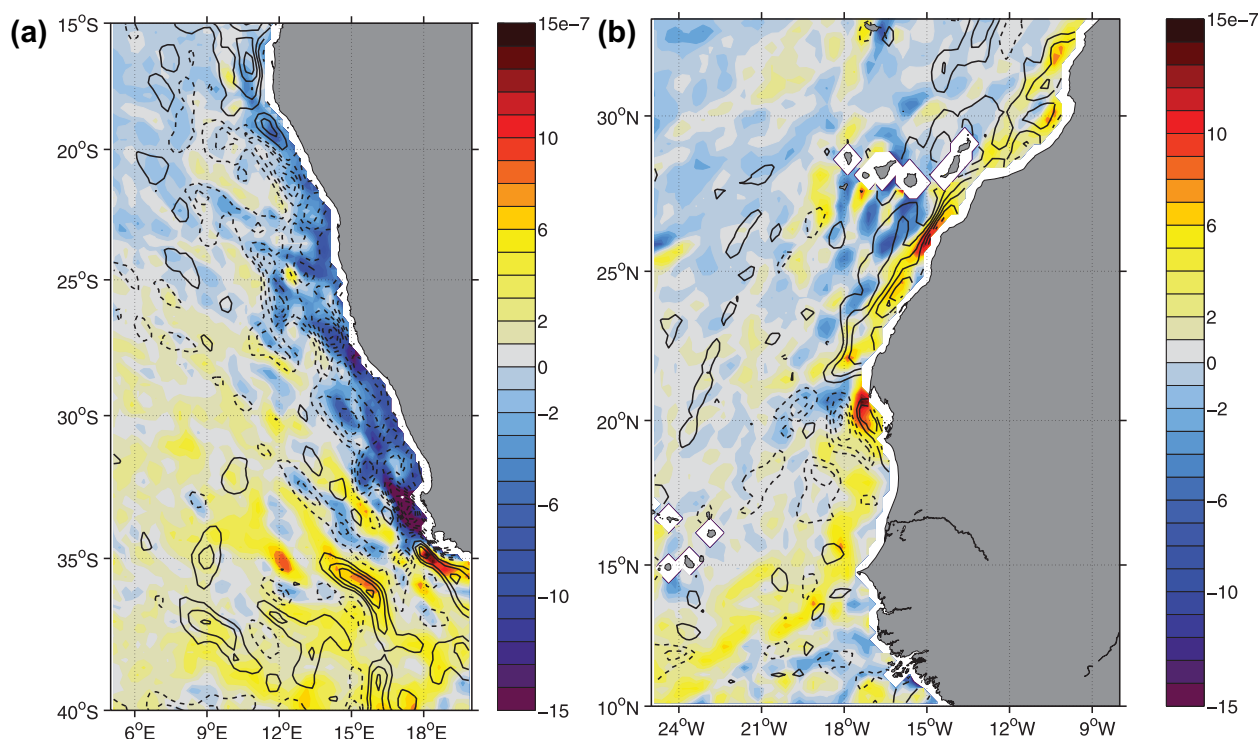
Figure 2. Seven day running mean of wind stress curl (color, in Pa/m) and crosswind SST gradient (contours, with a $5 \cdot \times 10^{-5}°$C/m interval and dashed negative values). (a) 12 February 2005 in the Benguela upwelling system. (b) 20 August 2005 in the Canary upwelling system.

side, which produces either negative or positive wind stress curl (depending on the wind direction) [O'Neill et al., 2005]. At seasonal time scales and during summertime, the patterns of wind stress curl and crosswind SST gradient are significantly linked in both upwelling systems (Figures 1b and 1d). The adjustment of the wind speed over the cross-shore SST gradient gives rise to upwelling-favorable cyclonic curl in both upwelling systems (i.e., positive curl for the Northern Hemisphere and negative curl for the Southern Hemisphere).

Figure 2 shows the 7 day running-mean wind stress curl and crosswind SST gradient for a specific date during the upwelling season in the Southern Benguela and Northern Canary systems. In the examples presented here, i.e., 12 February 2005 and 20 August 2005 for the Benguela and Canary upwelling systems, respectively, the synoptic situation corresponds to fully developed upwelling conditions with strong alongshore wind stress off the whole coastal Benguela and Northern Canary domains (not shown). The steady direction of the wind forces a strong SST front over the coastal domain. In return, the SST feeds back on the wind field in evolving specific wind stress curl structures. Indeed, in the cases shown in Figure 2, the spatial organization of the curl is well correlated with the crosswind component of the SST gradient: in the coastal band, the small-scale structures of the wind stress curl and the mesoscale SST perturbations (meanders and eddies) are well matched.

3.3. Linear Regression and Coupling Coefficient
As reported by Chelton et al. [2007], the links between SST and winds in the California upwelling system highlight a linear relationship between the wind stress curl and the crosswind SST gradient. In the Benguela and Canary systems, we statistically evaluate the response of the wind stress curl to SST by bin averaging the 7 day running means of the QuikSCAT wind stress curl observations as a function of the 7 day running means of the crosswind SST gradients over the full analysis period.

Figure 3 shows the standard deviation (red bars) and mean value (green line) of collocated 7 day running means of the wind stress curl and crosswind SST gradient in various computational domains in the Benguela system. The sensitivity of the results to the spatial domain is studied by either keeping all the grid points of the analysis, or taking only the grid points over the continental shelf (ocean depths within 0–500 m), over the coastal fringe (∼25 to 100 km from the coast), or over the expected upwelling extension
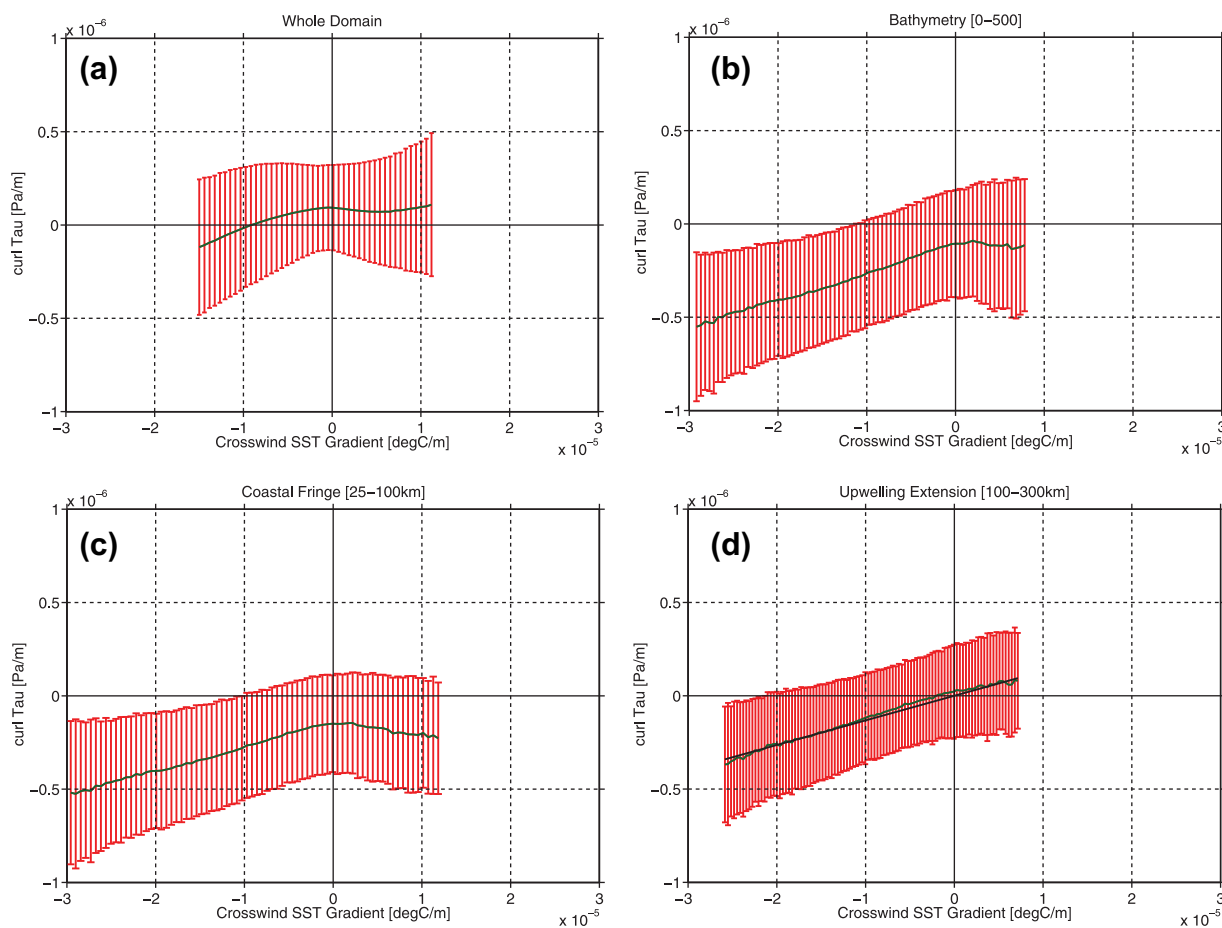
Figure 3. Binned scatterplot of the full time series of 7 day running means of wind stress curl and crosswind SST gradient over (a) the whole domain, (b) the continental shelf (for ocean depths less than 500 m), (c) the coastal fringe (∼25–100 km from the coast), and (d) the upwelling extension zone (100–300 km) for the Benguela system. The red bars indicate plus and minus one standard deviation about the average drawn with a green line. The linear regression from which the coupling coefficient is derived (see discussion in the text) is shown with a black line in Figure 3d and is calculated over the central 95% of the distribution.

(∼100 to 300 km). Our analysis strongly suggests that a linear regression only makes sense over the upwelling extension. The thermal coupling is a major process at work there: the wind stress curl tends to be linearly related to, and positively correlated with, the crosswind SST gradient, either with negative or positive crosswind SST gradients; this is not the case for the other areas. This result corroborates the hypothesis that wind perturbations induced by SST mesoscale variability predominate in the upwelling extension zone, knowing that the largest part of oceanic mesoscale dynamics in EBUS is confined in this coastal band [*Marchesiello et al.*, 2003]. In the same manner as *O'Neill et al.* [2005], the slope of the linear regression of the binned scatter plot (0.013, see Table 2) is hereafter referred to as the coupling coefficient (α_c). Unlike *Chelton et al.* [2007], the overlapping 7 day curls and crosswind SST gradients are here calculated from spatially unfiltered fields. The time-averaging window looks sufficient to remove the synoptic noise and bring out the SST influence on the wind [*Boé et al.*, 2011] (see section 6). The 7 day running-mean wind stress curl and crosswind SST gradient in the Benguela and the Canaries systems show discernible curl mesoscale features (see Figure 2).
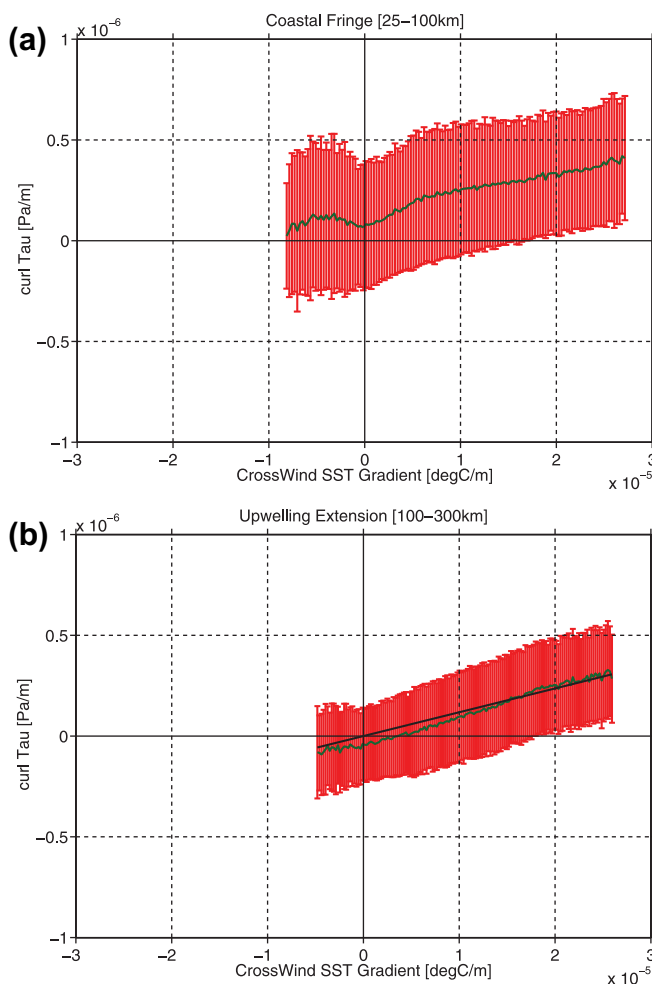
It is worth noting that other computational domains do not lead to good linear relationships between crosswind SST gradients and wind stress curls, in particular with regard to weak curl values in the coastal fringe. There, orographic constraints or local atmospheric dynamics add to the thermal coupling to shape the wind stress curl. In the Benguela upwelling system, atmospheric synoptic conditions (see section 3.1) and the land-sea transition lead to prevailing negative wind stress curl over the oceanic coastal fringe. The shift of the mean (green line in Figure 3c) from the origin can be interpreted as the effect of other factors besides thermal coupling (e.g., local atmospheric forcing, dropoff, orographic and coastline effects).

Table 2. Dependence of the Coupling Coefficient (Expressed in N·m^{-3}·(°C)$^{-1}$) on the Period Used for Its Estimation[a]

		Region		
		Benguela (Upw. Ext. Zone)	Northern Canary (Upw. Ext. Zone)	Southern Canary (Coastal Fringe)
Period	Summertime	0.017	0.016	0.011
	Wintertime	0.011	0.010	0.014
	Full series	0.013	0.011	0.013

[a]The results are given for the whole Benguela system and the Northern Canary system (21°N–25°N) over the upwelling extension zone (i.e., between 100 and 300 km from the coast), and for the coastal fringe (∼25–100 km) of the Southern Canary system (15°N–19°N). The coupling coefficient is estimated with the central 95% of the distribution of the crosswind SST gradient.
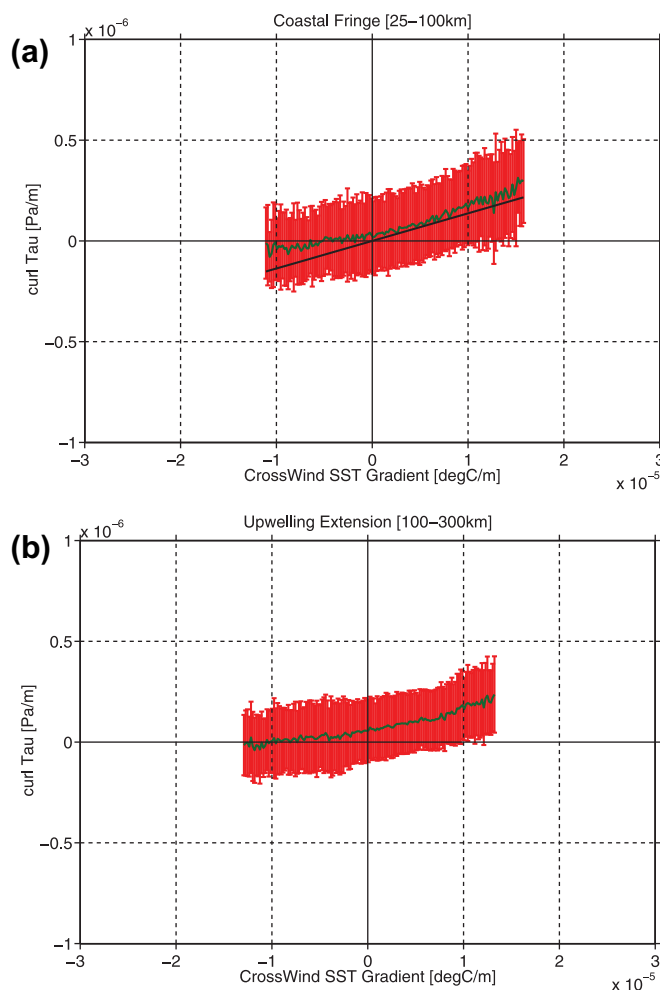
The evidence of an active oceanic feedback on low-level winds depends on the structure of the wind itself and requires little variability in its direction [*O'Neill et al.*, 2012; *Castelao*, 2012]. The Canary upwelling system differs from the Benguela system in more fluctuating wind directions. Indeed, the wind stress directional steadiness, defined by *Castelao* [2012] as the magnitude of the average wind stress vector divided by the scalar average of the wind stress magnitude, is weaker in the Canary system (not shown). The wind variability is also conditioned by the presence of islands, which complicates the relationship between the wind stress curl and crosswind SST gradient. Knowing the sensitivity of the coupling process to the wind directional steadiness, we choose to consider here the Northern Canary (from 21°N to 25°N) and the Southern Canary (from 15°N to 19°N) areas where the wind is not too much variable. The analysis of the bin-averaged scatterplot of the wind stress curl and crosswind SST gradient is shown in Figures 4 and 5, for the Northern and the Southern Canary systems, respectively, this time only for the coastal fringe and upwelling extension.

The Northern Canary region gives similar results to the Benguela system. This is not surprising because this area is characterized by upwelling-favorable winds throughout the year, by the presence of an extended SST front (not shown) and by the plausible orographic influence of the Atlas Mountains. Thus, the wind stress curl and crosswind SST gradient are linked linearly in the upwelling extension zone, as opposed to the coastal fringe where other processes

Figure 4. Binned scatterplot of the full time series of 7 day running means of wind stress curl and crosswind SST gradient over (a) the coastal fringe (∼25–100 km from the coast) and (b) the upwelling extension zone (100–300 km) for the Northern Canary system (from 21°N to 25°N). The red bars indicate plus and minus one standard deviation about the average drawn with a green line. The linear regression from which the coupling coefficient is derived is shown with a black line in Figure 4b and is calculated over the central 95% of the distribution.

Figure 5. Same as Figure 4 but for the Southern Canary system (from 15°N to 19°N). The linear regression from which the coupling coefficient discussed in the text is derived is shown with a black line in (a) and is calculated over the central 95% of the distribution.

seem to prevail in the shaping of the curl. On the other hand, unlike the Northern Canary and Benguela systems, a more direct relationship between the wind stress curl and crosswind SST gradient is discernable in the coastal fringe of the Southern Canary region (Figure 5a). This can be explained by two features: first, the SST front that develops during the upwelling season is located closer to the coast; second, the absence of any orographic barrier allows better and easier evidence of the thermal coupling. In the other regions we analyzed, our working hypothesis is that the coupling between SST and the wind stress curl may exist in the coastal fringe, but is not the main process that drives wind stress curl variability.

The soundness of the coupling coefficient found for the different regions is verified by studying its sensitivity to different time parameters (Table 2). This sensitivity refers to contrasted periods of analysis: summertime, wintertime and the 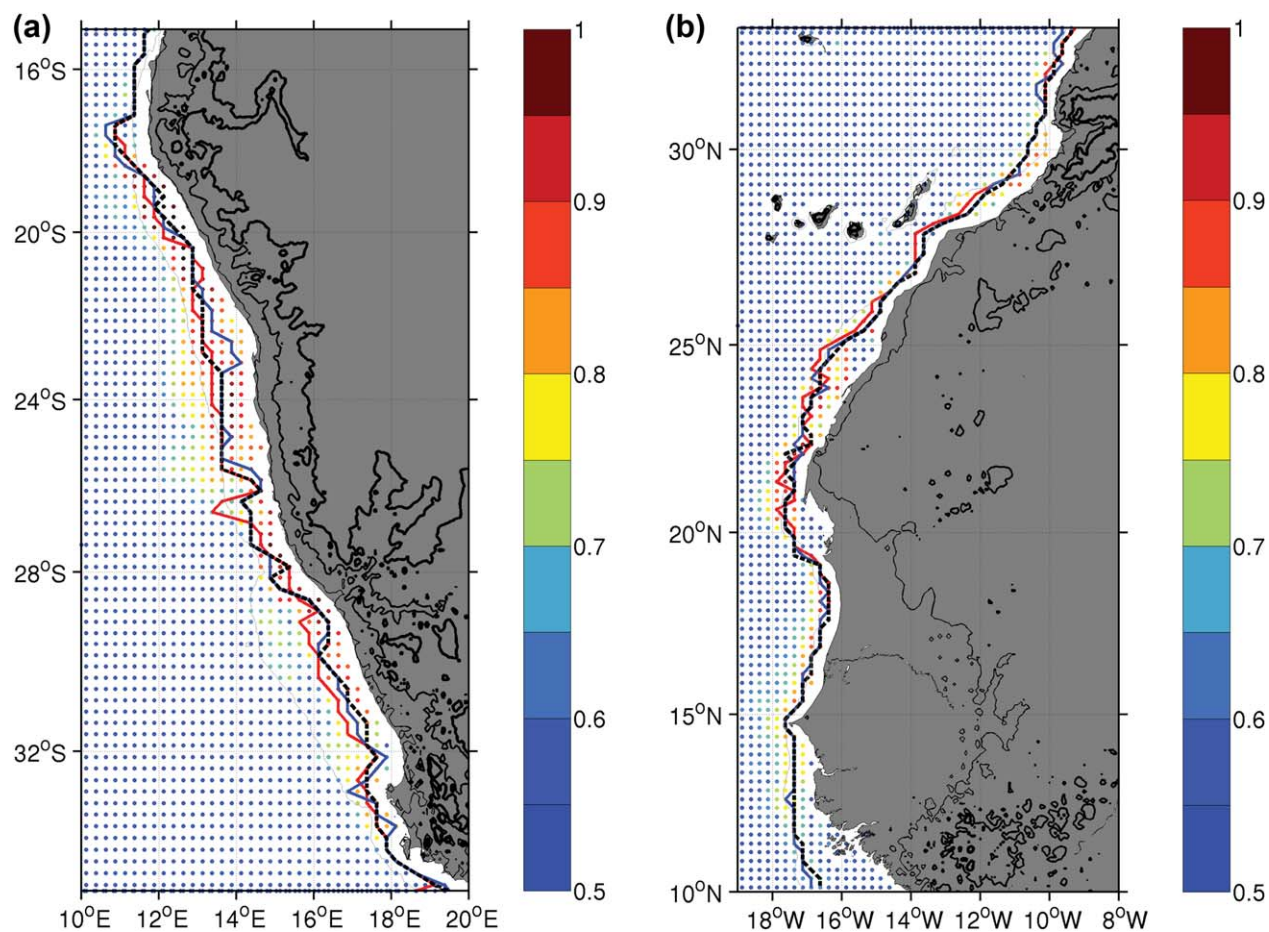entire time series. The largest coefficients are obtained in summer (winter), for the Benguela and Northern Canary systems (Southern Canary system), which suggests that the coupling process is more efficient during an upwelling season (see also section 4). The thermal coupling coefficient between the wind stress curl and crosswind SST gradient is strongly dependent on the wind direction steadiness, which is more established during the upwelling season than during periods of wind relaxation (not shown).

4. Local Analysis of the SST-Driven Curl Variability and Magnitude

As discussed in the previous section, the weekly averaged wind stress curl shows dependence on the crosswind SST gradient with a positive coupling coefficient, in both upwelling systems. Therefore, when this oceanic feedback is active and dominant, the two fields should have locally the same sign. This is why we calculate the percentage of curl events that satisfy this property, i.e., same signs of QS25 wind stress curl and crosswind Reynolds SST gradient, over the full 5 year time series (Figure 6). In order to check the consistency of the linear model that links SST and the wind, we focus at each latitude on the reference grid point that captures the maximum percentage of same sign wind stress curl and crosswind SST gradient. For this purpose, Figure 6 also shows at each latitude the locations of these reference grid points for an analysis focused on winter months (blue line) or summer months (red line), or done over the full time series (dashed black line). The latter line is usually found in the upwelling extension zone, matching the mean position of the SST front where the SST feedback is likely active most of the time. Indeed, the percentage of curl events associated with a crosswind SST gradient of the same sign shows marked contrasts in the cross-shore direction: the closer to the coast, the lesser percentage (see colored values in Figure 6).

Figure 6. Percentage of days with equal signs for wind stress curl and crosswind SST gradient (colored dots) and, for each latitude, location of the maximum percentage for an analysis focused on winter months (blue line), summer months (red line), or calculated over the full time series (dashed black line). (a) For the Benguela upwelling system. (b) For the Canary upwelling system. The black lines over land show the 100, 500, and 1000 m elevations above sea level and the gray thin line shows the 500 m isobath.

Several processes may explain the occurrence of opposite signs for both analyzed quantities. First, the upwelling cell can be located quite offshore in the presence of a broad shallow shelf [*Estrade et al.*, 2008], and a reverse coastward SST gradient can develop locally under anticyclonic, upwelling-favorable wind conditions (for example, downwind Cape Blanc; see Figure 1d and *Estrade et al.* [2008]). Then, the sign of the wind stress curl can be set by other factors than the local SST feedback. This is typically the case in the thin coastal band where orographic effects complicate the relationship between the curl and the crosswind SST gradient [*Boé et al.*, 2011]. This process is expected to be even stronger if the continental orography is pronounced. This result is confirmed in the Northern Canary upwelling system where the detachment from the coast of the maximum of the percentage of equivalent signs is important in the latitude range of the Atlas Mountains (between 22°N and 33°N; on the continent, the black bold line in Figure 6 shows the 100 m height above the sea level). On the contrary, this detachment is not visible in the Southern Canary area where the maximum of percentage is reached at the first unmasked ocean grid point (between 14°N and 18°N). This result confirms the analysis of the regression between the two fields (see section 3.3). Downwind Cape Blanc (20°N), the signs of the wind stress curl and crosswind SST gradient are also most often unrelated, and the maximum of percentage of equivalent signs is located far offshore whatever the season (Figure 6b). The atmospheric wind field in this area is highly constrained by the cape. In this matter, the Benguela system differentiates itself from the Canary system because it corresponds to quite a homogeneous continental orography along the shoreline (black bold line in Figure 6a). Thus, the percentage of equivalent signs between the wind stress curl and the crosswind SST gradient shows an onshore decrease at almost every latitude except north of 18°S.

We aim at assessing the relative contribution of the SST-driven curl to the total wind stress curl derived from QuikSCAT observations. For that purpose, we calculate each day the percentage of the curl related to SST as expressed by:

$$P_{explained} = 100 \, \alpha_c |\nabla SST| \sin \theta / |\nabla \times \tau|$$

In this estimate, the coupling coefficient is chosen to be a constant and corresponds to the value found for the entire time series in both the Benguela and Southern Canary systems (see Table 1), i.e., $\alpha_c = 0.013$ N·m^{-3}·(°C)$^{-1}$. Therefore, we recognize that the explained percentage will be underestimated during the dominant upwelling season and overestimated during the relaxation period. Our purpose is simply to diagnose and verify if the wind stress curl ascribed to SST spatial variability is of the same order of magnitude as the total curl derived from QuikSCAT. In this way, time series of the relative contribution of SST-driven curl to total wind stress curl can be calculated locally. By construction, these time series of percentage show only positive values. The largest values may however exceed unity (i.e., 100%) because the curl calculated from the local crosswind SST gradient can exceed the QuikSCAT curl.

For each latitude and for both upwelling systems, Figure 7 shows the distribution of $P_{explained}$ at the reference grid point identified by the black dashed line in Figure 6. The colors refer to the percentage of events belonging to each 5% bin considered for $P_{explained}$. A wide range of values is obtained for $P_{explained}$ (from 0 to up to 250%). At some latitudes and at given times, the curl calculated from the local crosswind SST gradient can be more than twice as large as the QuikSCAT curl. One can assume that during these specifics events (that are not representative of the average conditions), pure internal atmospheric variability tends to reduce locally the observed curl. In contrast, at some latitudes, the SST-driven curl makes always a negligible contribution to the total wind stress curl, with reduced $P_{explained}$ values. This is notably the case just south of 20°N and everywhere south of 14°N in the Canary upwelling system, and around 33°S in the Benguela system. In these locations, the distribution of $P_{explained}$ is much less symmetric and peaks for values close to zero. These latitudes correspond to the locations of major capes (Cape Ghir, Cape Blanc, and Cape Verde for the Canary region, and Cape Columbine for the Benguela region). We can argue here that the rugged coastal area is the main factor responsible for curl variability and, thus, that the SST distribution explains only a negligible fraction of the total curl magnitude. The distribution shape of the explained percentage is nearly Gaussian at the other latitudes, and the percentage at its peak value shows that the SST-induced curl is a primary contributor to the local curl variability and magnitude.

The sensitivity of the explained percentage to the period over which the coupling coefficient is computed is worth investigating. To evade the difficulty of reference grid points too closely related to a specific period of the year, the distributions of explained percentage are now averaged zonally over the domain encompassed by the blue, red and dashed black lines drawn in Figure 6. Furthermore, for the sake of brevity, the focus is on the median value of each averaged distribution, as displayed in Figure 8 as a function of latitude for both the Benguela and Canary upwelling systems. South of 28°S, the contribution of the SST-driven curl to the total curl during summertime is larger than during wintertime (see Figure 8a). North of this latitude, the seasonal contrasts are weaker. Indeed, in the Southern Benguela system, the favored season for offshore Ekman transport and, thus, strong upwelling dynamics is summer (see section 3.1), whereas the Northern Benguela system is characterized by almost permanent upwelling conditions. North of 18°S, in the region of the Angola-Benguela front, the SST-driven curl is more efficient during summertime than during wintertime. As the analysis is done on the first unmasked ocean grid point (see Figure 6a), we can theorize that orographic and local atmospheric effects are the main drivers for the curl in winter, knowing that the wind stress is larger during this season (not shown). In the Canary upwelling system (Figure 8b), the relative contribution of the SST-induced curl to the total curl during wintertime (the upwelling-favorable season for the Southern Canary region) is significantly larger south of 18°N, and slightly smaller north of 22°N, than the relative contribution calculated over summer months. Around 20°N, the calculation of the median shows weak sensitivity to the reference period, which is not unexpected given the almost persistence of the upwelling process at these latitudes (see section 3.1). These results show that the contribution of the SST-induced curl is season dependent and back up the conclusions of our sensitivity study carried out on the magnitude of the coupling coefficient (see section 3.3). It is important to remind here that the method used a unique and constant coefficient for both systems and for all the seasons. This assumption does not reflect the seasonal and spatial dependence of the SST-wind stress interactions. Yet, the error attributable to the use of a constant coefficient (shaded areas in Figure 8) does not change the order of magnitude of the
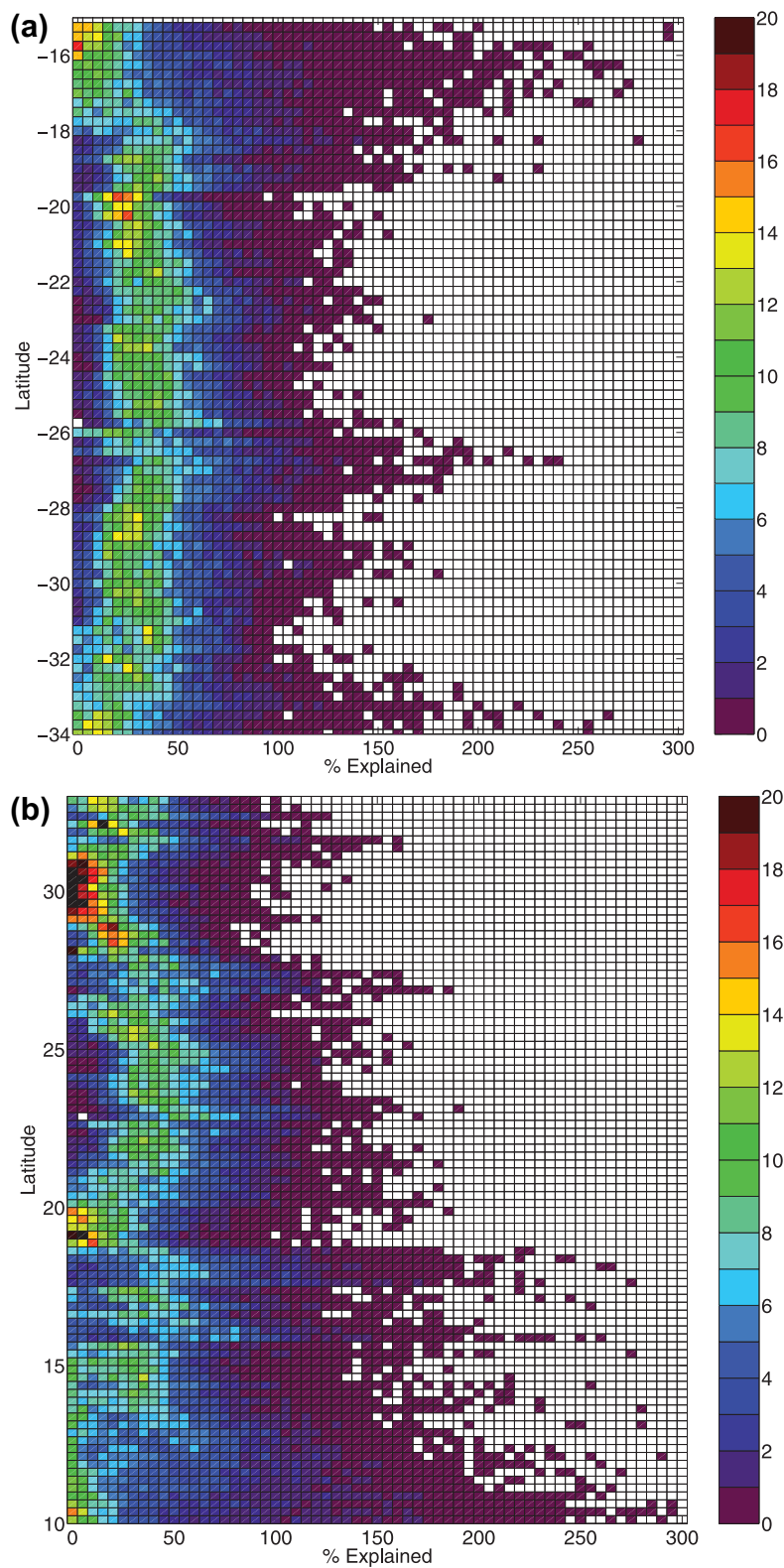
Figure 7. Fraction (expressed as a percentage) of the local wind stress curl explained by SST-driven curl. The distribution is calculated over the full time series and is shown as a function of latitude at the reference points identified with the black dashed line in Figure 6 (see details in the text). (a) For the Benguela upwelling system. (b) For the Canary upwelling system.
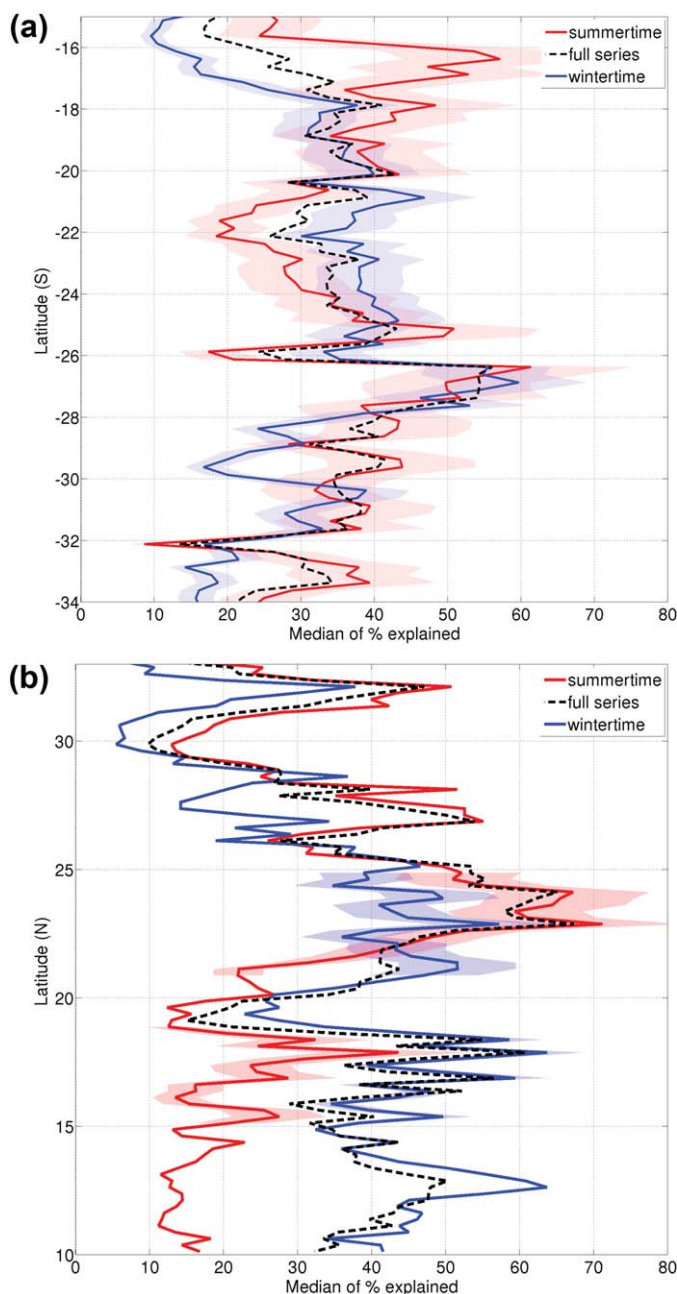
Figure 8. Median values of the zonally averaged distributions of explained percentage of curl, with the average calculated at each latitude over the area encompassed by the blue, red, and dashed black lines defined in Figure 6. (a) For the Benguela upwelling system. (b) For the Canary upwelling system. The shaded area shows the error associated with the use of a constant and unique coupling coefficient instead of a regional and seasonal estimate (see Table 2).

median value of $P_{explained}$. The region north of 30°N is characterized by significant SST-driven curl during summer, plausibly related to the regular presence of the Cape Ghir upwelling filament [*Troupin et al.*, 2012]. South of the cape, the roughness of the coastal area drives wind variability and, thus, local atmospheric effects are the primary contributor to wind stress curl variability and magnitude.

5. QS25/QS50 Comparison

In the previous sections, QS25 winds were shown to be sensitive to the SST: they tend to decelerate over colder SST, with implications for wind stress curl patterns over the whole extension of the upwelling. The sensitivity is more subtle in the nearshore ocean where coastal promontories and orographic effects become more important. Here we compare the QS25 wind stress field to the former QS50 product.

Figure 9 shows the horizontal gradients of the 7 day running-mean wind stress magnitude and SST on the same day as presented in Figure 2a for the Benguela upwelling system, for the two QS25 and QS50 products. When an oceanic feedback is active on low-level winds, the structure of the wind stress gradient roughly matches that of the SST gradient because of the accentuation of the wind stress curl.
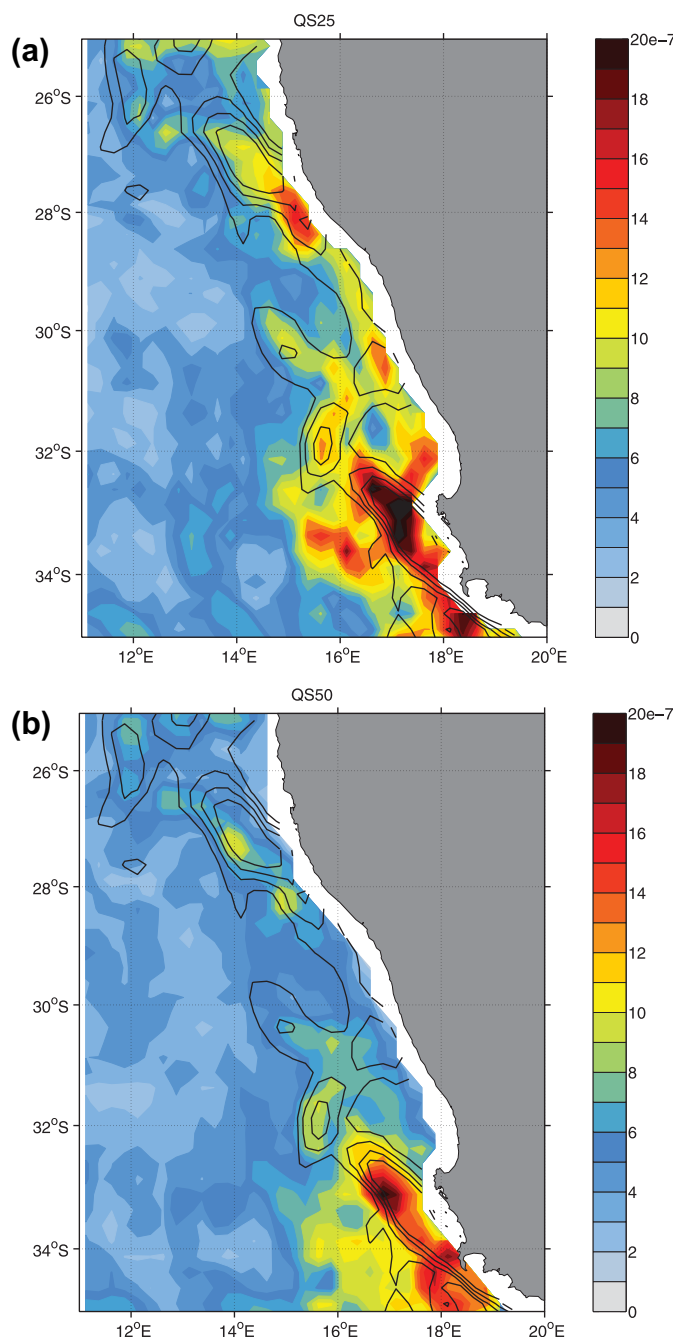
Figure 9 provides strong indication that the QS50 wind stress modification is less intense than its QS25 counterpart for a same value of the SST gradient. In this example, the wind stress modification corresponds mostly to an intensity reduction (see Figure 2b) with, as a result, larger wind stress curl values in QS25 than in QS50. Indeed, the main differences are found in the coastal domain where strong SST gradients develop (black contours in Figure 9). In other words, the QS50 wind magnitude exceeds the QS25 magnitude where a deceleration of the wind is expected because of an active SST feedback. This strongly suggests that the QS50 product accounts more poorly for SST-wind interaction in the coastal band of an upwelling system. We also calculated the slope of the regression line between the QS25 and QS50 wind stress gradients

Figure 9. Seven day running mean of wind stress magnitude gradient (color, in Pa/m) for the date introduced in Figure 2a for the Benguela system (i.e., 12 February 2005). For (a) the QS25 product and (b) the QS50 product. The SST gradient is superimposed with black contours (with a $5 \cdot \times 10^{-5 \circ}$C/m interval) and is the same in both plots.

considered over the patches of SST gradients stronger than a given threshold to check that a quantitative analysis based on the full time series confirms and generalizes the differences exemplified in Figure 9 (not shown).

The differences between both wind products can also be shown by a joint analysis of the wind stress curl and crosswind SST gradient over the upwelling extension zone of the Benguela system, in a way similar to what we did with the QS25 product (see section 3.3) and using a crosswind SST gradient specific to each wind product. A linear regression over the upwelling extension zone and for the full time series does not appear to be valid for the QS50 product, especially for low and positive values of the crosswind SST gradient (not shown). The coefficient of determination (R^2) can here be used to study the quality of the linear models that best fit the two distributions. Table 3 reports the coupling coefficients and corresponding R^2 values for extended calculations over the upwelling extension zone of the Benguela and Northern Canary systems, and over the coastal fringe of the Southern Canary system. Though the direct comparison of the coupling coefficients is a hard task, especially because of their time and space dependence and because of the absence of published reference values for these upwelling regions, it is worth noting that the coupling coefficient is always more important with the high-resolution wind stress product (QS25). These statistics confirm the result proposed in Figure 9 for a specific day in the Benguela region. The R^2 coefficients obtained for QS25 are also larger than for QS5, which suggests that the QS25 wind field samples the wind stress curl attributable to the air-sea coupling better than the former QS50 product. It is still worth noting that the QS50 wind stress is not totally blind to patterns inherent to the air-sea coupling: gradients of wind stress magnitude and gradients of SST can appear partly collocated (Figure 9b).

Table 3. Coupling Coefficients (Expressed in $N \cdot m^{-3} \cdot (°C)^{-1}$) Estimated From the Full Time Series of the QS25 and QS50 Products, and Corresponding R^2 Coefficients[a]

		Coupling Coefficient	R^2
Benguela	QS25	0.013	0.89
(upw. ext. zone)	QS50	0.012	0.62
Northern Canary	QS25	0.011	0.67
(upw. ext. zone)	QS50	0.008	0.55
Southern Canary	QS25	0.013	0.85
(coastal fringe)	QS50	0.010	0.53

[a]The results are given for the whole Benguela system and the Northern Canary system (21°N–25°N) over the upwelling extension zone (i.e., between 100 and 300 km from the coast), and for the coastal fringe (∼25–100 km) of the Southern Canary system (15°N–19°N). The coupling coefficient is estimated with the central 95% of the distribution of the crosswind SST gradient.

6. Discussion and Concluding Remarks

In this study, high-resolution wind stress fields derived from QuikSCAT measurements and SST data gridded at 1/4° were used to investigate SST-induced wind stress curl patterns at weekly time scales in both the Benguela and Canary upwelling systems. We verified a positive correlation where the upwelling SST front is visible, with a linear response of the wind stress curl to a crosswind SST gradient over both systems. The analysis of 5 full years of 7 days running means of QuikSCAT wind stress curl and crosswind Reynolds SST gradient showed that the general scheme suggested by *Chelton et al*. [2004] and

O'Neill et al. [2005] is respected for the SST and wind stress curl observed off the western African coast (section 3). Nevertheless, we showed that the linear model that connects the crosswind SST gradient and the wind stress curl was not to be applied everywhere from the coast to the upwelling extension (where the SST gradient is large and to a certain extent steady). Close to the shore, the curl patterns derived from QuikSCAT wind observations are only loosely related to SST-wind interactions. We interpret this as the signature of the coastline geometry and orographic effects (sections 3 and 4). We also quantified the part of the wind stress curl that could be explained by the SST spatial variability with the use of a constant coupling coefficient (section 4). The SST-driven curl can be an important contributor to the local wind stress curl variability and magnitude (with median values for the explained fraction of the curl up to 60% locally during the main upwelling season), noting that the total wind stress curl is almost unrelated to the crosswind SST gradient close to coastal promontories. The strength of the SST-wind interaction also depends on the season, with a larger coupling during upwelling-favorable months. Lastly, a simple comparison of the high-resolution QS25 product with the former coarser-resolution QS50 product shows that the expected linear relationship between the crosswind SST gradient and wind stress curl is less apparent with the older wind product. Moreover, the atmospheric signature of an SST gradient is systematically greater in the QS25 product, in terms of wind reduction and, thus, wind stress curl magnitude.

Since the ocean and the atmosphere form a closely interacting system over a large spectrum of variability and, moreover, through numerous processes, the clear identification of the time scales at play and the assessment of the causes and effects of the reciprocal forcing are a hard task. Indeed, as noted by *Wallace et al*. [1990] for extratropical regions, two-way simultaneous relationships based on monthly data may contain both directions of forcing since the ocean mixed layer responds to atmospheric events on a time scale of days to months, while the atmosphere should respond within a week. *Chelton et al*. [2007] discussed the length of the averaging period needed to highlight the SST feedbacks on the low-level wind in the California upwelling system. They showed that air-sea coupling was clear with averages of 10 days or more. In our present study, the feedback on wind could be investigated with 7 day running-mean fields, especially during the upwelling season when a sharp SST front develops in the Benguela and Canary systems. We acknowledge that, on this time scale, the wind stress curl also forces the SST variability through Ekman pumping. A lagged correlation analysis between the wind stress curl and crosswind SST gradient indicates that, from 1 to 30 day averaging windows, the maximum of correlation is obtained at lag 0, with more rounded profiles for larger windows (not shown). The latter observation echoes the results obtained by *Chelton et al*., [2007] for the California system (see the top panel of their Figure 12). Starting from 7 days, the asymmetry of the correlation profiles becomes important: the correlations for negative lags are larger than for equivalent positive lags, which means that the wind stress curls are better correlated with earlier crosswind SST gradients than with later gradients. This suggests that the crosswind SST gradient is a source of forcing for the wind stress curl. The atmospheric forcing by SST is confirmed by the positive correlation between the wind stress and SST at this time scale (not shown). On time scales longer than 7 days, the one-way forcing becomes even more obvious [*Chelton et al*., 2007].

The efficiency of the SST feedback on the low-level winds was shown to be season and space dependent. The time sensitivity is not surprising since the linear relationship suggests that the SST-driven wind curl is stronger for a sharper crosswind SST gradient and since the coastal water temperature is largely controlled by the seasonality of the offshore Ekman transport. Moreover, as suggested by *Chelton et al.* [2007] and *Castelao* [2012], steadiness of the wind is an important condition for the completion of the SST feedback. The latter point can explain the time sensitivity identified in both the Benguela and Canary systems, considering that the wind direction is steady enough during the upwelling season to allow achievement of the full process. In addition, we have seen that the coupling coefficient is generally weaker in the Canary system than in the Benguela region. The orographic forcing induced by the Canary Islands on the wind stress and wind stress curl variability [*Chelton et al.*, 2004] may disrupt the completion of the full coupling process.

The coupling coefficients calculated during upwelling-favorable conditions in both the Benguela and Canary systems have values close to, but weaker than, those calculated during summertime in the California region by *Chelton et al.* [2007], though with different data sets. The Reynolds SST used in this study differs from the AMSR-E observations used for their California study by its higher resolution. Moreover, the blind zone around the coast of the QS25 wind stress field distributed by CERSAT does not exceed 30 km and, in our study, the wind stress curl and crosswind SST gradient can be calculated from approximately 50 km from the shoreline. Therefore, our interpretation of an orographic imprint in the coupling process is backed up by the fact that this effect may exist more than 100 km offshore [*Boé et al.*, 2011]. We are confident that the onshore decrease of the coupling between the wind stress curl and crosswind SST gradient is soundly grounded (as diagnosed from the sign and percentage of the explained contribution of SST-induced curl to the total curl). Both fields are even less related close to a coastal cape or to local strong continental orography (i.e., the proximity of the Atlas Mountains; see Figure 6b).

The thermal coupling is not fully discussed in this study since the relationship between the downwind SST gradient and wind stress divergence and the relationship between the SST and wind stress themselves are not investigated. We deliberately focused on the coupling between the wind stress curl and crosswind SST gradient because it is pertinent for modeling oceanic studies that use QuikSCAT products as a forcing function, knowing that the wind curl is a determinant factor for near-surface dynamics in EBUS [e.g., *Capet et al.*, 2004; *Münchow*, 2000]. We pointed out that the Ekman dynamics driven by the wind stress curl develops in different ways in the cross-shore direction because of SST-wind coupling (over SST gradients) and orographic effects, in particular in the Benguela and Northern Canary upwelling systems. Within about 100 km of the coast, SST gradients do affect the variability of the wind stress curl, but less than a rugged coastal area or orography. In contrast, from 100 km and beyond, SST gradients are the main driver for the curl. From an ocean modeling point of view, the QS25 data set, with its improved effective spatial resolution, turns out to be a suitable product for the investigation of small-scale variability over the shelf in an upwelling system because it was shown to capture at least part of this cross-shore variability. Equivalently, it is worth noting that atmospheric models run with the aim to simulate realistic winds in upwelling systems must rely on high-resolution SST, especially where SST fronts meander and ocean mesoscale dynamics are important. The existence of a blind zone in scatterometer coverage (a few tens of kilometers) is still a strong limitation over the inner shelf since regional ocean models are now run at a resolution equal or sharper than a few kilometers, thus with ocean grids cells lying in this blind zone. New generation analysis products (e.g., from the European Center for Medium-Range Weather Forecasts; see http://www.ecmwf.int/en/forecasts/documentation-and-support/changes-ecmwf-model/cy40r1-summary-changes) are now distributed on a spatial grid that seems appropriate for the identification of such near-coastal processes, but they are unfortunately available only over short or recent periods. In our mind, a rewarding strategy for EBUS modeling will likely merge observational data from high-resolution scatterometer and small-scale structures deduced from model analyses (notwithstanding the possibility of spurious Gibbs oscillations stemming from the truncated spectral representation of the earth's topography and, thus, of the drag coefficient), looking forward to obtaining new generation satellite winds as close as a few kilometers from the coast (e.g., RapidSCAT; see *Rodríguez* [2013] and http://winds.jpl.nasa.gov/missions/RapidScat/). Indeed, the full feedback loop between the SST distribution, wind stress curl and Ekman-induced pumping cannot be disentangled based on 2-D satellite observations alone. Its quantification in numerical three-dimensional models is an important issue, knowing that fully coupled regional simulations usually underestimate the influence of SST on the wind stress [*Boé et al.*, 2011]. It is worth reminding here that, with an empirical

coupled model, *Jin et al.* [2009] showed that this process affects strongly SST (they obtained warmer surface conditions for the coupled mode), and thus the entire coastal upwelling dynamics. Then, the dynamical coupling between the wind stress and oceanic currents can be important in EBUS. More information is needed to suitably tackle this issue, and future satellite missions that aim to sample collocated currents and 10 m neutral winds will likely prove decisive for this purpose.

The QS25 product stems from a new algorithm dedicated to the complete utilization of the SeaWinds scatterometer samples, whereas the former QS50 winds were provided at half-degree horizontal resolution and did not use the full potential of the satellite swaths. Moreover, QS50 and QS25 estimates are based on the use of the *Smith* [1988] and *Fairall et al.* [2011] parameterizations, respectively. The two parameterizations have been commonly compared using in situ data as a reference [e.g., *Drennan et al.*, 2003]. It is still worth noting that the COARE3.0 parameterization [*Fairall et al.*, 2011] relies on *Smith* [1988] for mean conditions, and the spatial distribution of the relative mean difference between the wind stresses estimated with the two parameterizations is quite small. Moreover, the COARE3.0 wind stress estimates are much more sensitive to the wind speed than to SST (not shown). We show in this study that the QS50 winds are less statistically related to the SST field than the QS25 winds. Therefore, the QS25 data include spatial scales that are coherent with the scales of coupled thermodynamical processes between the wind and SST. The large difference in stress magnitude associated with the neglect of these scales can lead to overestimation of coastal upwelling when forcing a model with coarse-resolution QuikSCAT winds, as pointed out by *Burls and Reason* [2008]. In this framework, the careful comparison of the response of a numerical regional model to winds as different as QS25 and QS50 is a promising method to assess better the structure and intensity of the wind- and wind curl-driven upwelling dynamics.

References

Bentamy, A., and D. Croizé-Fillon (2011), Gridded surface wind fields from Metop/ASCAT measurements, *Int. J. Remote Sens.*, 33, 1729–1754, doi:10.1080/01431161.2011.600348.

Bentamy, A., S. A. Grodsky, K. Katsaros, A. M. Mestas-Nuñez, B. Blanke, and F. Desbiolles (2013), Improvement in air-sea flux estimates derived from satellite observations, *Int. J. Remote Sens.*, 34, 5243–5261, doi:10.1080/01431161.2013.787502.

Blanke, B., S. Speich, A. Bentamy, C. Roy, and B. Sow (2005), Modeling the structure and variability of the southern Benguela upwelling using QuikSCAT wind forcing, *J. Geophys. Res.*, 110, C07018, doi:10.1029/2004JC002529.

Boé, J., A. Hall, F. Colas, J. C. McWilliams, X. Qu, J. Kurian, and S. B. Kapnick (2011), What shapes mesoscale wind anomalies in coastal upwelling zones?, *Clim. Dyn.*, 36, 2037–2049, doi:10.1007/s00382-011-1058-5.

Burls, N., and C. J. C. Reason (2008), Modelling the sensitivity of coastal winds over the Southern Benguela upwelling system to different SST forcing, *J. Mar. Syst.*, 74, 561–584.

Businger, J. A., and W. J. Shaw (1984), The response of the marine boundary layer to mesoscale variations in sea-surface temperature, *Dyn. Atmos. Oceans*, 8, 267–281.

Capet, X. J., P. Marchesiello, and J. C. McWilliams (2004), Upwelling response to coastal wind profiles, *Geophys. Res. Lett.*, 31, L13311, doi:10.1029/2004GL020123.

Carr, M. E. (1998), A numerical study of the effect of periodic nutrient supply on pathways of carbon in a coastal upwelling regime, *J. Plankton Res.*, 20, 491–516.

Castelao, R. M. (2012), Sea surface temperature and wind stress curl variability near a cape, *J. Phys. Oceanogr.*, 42, 2073–2087.

Chang, P., and S. G. Philander (1994), A coupled ocean-atmosphere instability of relevance to the seasonal cycle, *J. Atmos. Sci.*, 51, 3627–3648.

Chelton, D. B., M. G. Schlax, M. H. Freilich, and R. F. Milliff (2004), Satellite measurements reveal persistent small-scale features in ocean winds, *Science*, 303, 978–983.

Chelton, D. B., M. G. Schlax, and R. M. Samelson (2007), Summertime coupling between sea surface temperature and wind stress in the California current system, *J. Phys. Oceanogr.*, 37, 495–517.

Colas, F., J. C. McWilliams, X. Capet, and J. Kurian (2012), Heat balance and eddies in the Peru-Chile current system, *Clim. Dyn.*, 39(1-2), 509–529.

Desbiolles, F., B. Blanke, and A. Bentamy (2014), Short-term upwelling events at the western African coast related to synoptic atmospheric structures as derived from satellite observations, *J. Geophys. Res. Oceans*, 119, 461–483, doi:10.1002/2013JC009278.

Drennan, W. M., H. C. Graber, D. Hauser, and C. Quentin (2003), On the wave age dependence of wind stress over pure wind seas, *J. Geophys. Res.*, 108(C3), 8062, doi:10.1029/200JC000715.

Duncombe Rae, C. M. (2005), A demonstration of the hydrographic partition of the Benguela upwelling ecosystem at 26°40′S, *Afr. J. Mar. Sci.*, 27, 617–628.

Estrade, P., P. Marchesiello, A. Colin de Verdière, and C. Roy (2008), Cross-shelf structure of coastal upwelling: A two–dimensional extension of Ekman's theory and a mechanism for inner shelf upwelling shut down, *J. Mar. Res.*, 66, 589–616.

Fairall, C. W., M. Yang, L. Bariteau, J. B. Edson, D. Helmig, W. McGillis, S. Pezoa, J. E. Hare, B. Huebert, and B. Blomquist (2011), Implementation of the Coupled Ocean-Atmosphere Response Experiment flux algorithm with CO_2, dimethyl sulfide, and O3, *J. Geophys. Res.*, 116, C00F09, doi:10.1029/2010JC006884.

Fairall, C. W., E. F. Bradley, J. E. Hare, A. A. Grachev, and J. B. Edson (2003), Bulk parameterization of air-sea fluxes: Updates and verification for the COARE algorithm, *J. Clim.*, 16, 571–591.

Fennel, W., T. Junker, M. Schmidt, and V. Mohrholz (2012), Response of the Benguela upwelling systems to spatial variations in the wind stress, *Cont. Shelf Res.*, 45, 65–67.

Fore, A. G., B. W. Stiles, A. H. Chau, B. A. Williams, R. S. Dunbar, and E. Rodríguez (2014), Point-wise wind retrieval and ambiguity removal improvements for the QuikSCAT climatological data set, *IEEE Transactions on Geoscience and Remote Sensing*, *52*(1), 51–59.

Gill, A. E. (1982), *Atmosphere-Ocean Dynamics*, 662 pp., Academic, San Diego, Calif.

Haack, T., D. Chelton, J. Pullen, J. D. Doyle, and M. Schlax (2008), Summertime influence of SST on surface wind stress off the U.S. West Coast from the U.S. Navy COAMPS model, *J. Phys. Oceanogr.*, *38*, 2414–2437.

Jin, X., C. Dong, J. Kurian, J. C. McWilliams, D. B. Chelton, and Z. Li (2009), SST-wind interaction in coastal upwelling: Oceanic simulation with empirical coupling, *J. Phys. Oceanogr.*, *39*, 2957–2970.

JPL (2006), *QuikScat Science Data Product User's Manual*, Version 3.0, D-18053, 91 pp., Jet Propul. Lab., Pasadena, Calif. [Available at http://podaac.jpl.nasa.gov/DATA CATALOG.].

Lathuilière, C., V. Echevin, and M. Lévy (2008), Seasonal and intraseasonal surface chlorophyll-a variability along the northwest African coast, *J. Geophys. Res.*, *113*, C05007, doi:10.1029/2007JC004433.

Marchesiello, P., and P. Estrade (2010), Upwelling limitation by geostrophic onshore flow, *J. Mar. Res.*, *68*, 37–62, doi:10.1357/002224010793079004.

Marchesiello, P., J. C. McWilliams, and A. Shchepetkin (2003), Equilibrium structure and dynamics of the California current system, *J. Phys. Oceanogr.*, *33*, 753–783.

Münchow, A. (2000), Wind stress curl forcing of the coastal ocean near Point Conception, California, *J. Phys. Oceanogr.*, *30*, 1265–1280.

O'Neill, L. W., D. B. Chelton, S. K. Esbensen, and F. J. Wentz (2005), High-resolution satellite observations of SST modification of the marine atmospheric boundary layer over the Agulhas Return Current, *J. Clim.*, *18*, 2706–2723.

O'Neill, L. W., D. B. Chelton, and S. K. Esbensen (2010), The effects of SST-induced surface wind speed and direction gradients on midlatitude surface vorticity and divergence, *J. Clim.*, *23*, 255–281.

O'Neill, L. W., D. B. Chelton, and S. K. Esbensen (2012), Covariability of Surface Wind and Stress Responses to Sea Surface Temperature Fronts, *J. Clim.*, *25*, 5916–5942, doi:10.1175/JCLI-D-11-00230.1.

Perlin, N., R. M. Samelson, and D. B Chelton (2004), Scatterometer and model wind and wind stress in the Oregon-Northern California coastal zone, *Mon. Weather Rev.*, *132*, 2110–2129.

Pickett, M. H., and J. D. Paduan (2003), Ekman transport and pumping in the California Current based on the U.S. Navy's high-resolution atmospheric model (COAMPS), *J. Geophys. Res.*, *108*(C10), 3327, doi:10.1029/2003JC001902.

Renault, L., B. Dewitte, M. Falvey, R. Garreaud, V. Echevin, and F. Bonjean (2009), Impact of atmospheric coastal jet off central Chile on sea surface temperature from satellite observation (2000–2007), *J. Geophys. Res.*, *114*, C08006, doi:10.1029/2008JC005053.

Renault, L., B. Dewitte, P. Marchesiello, S. Illig, V. Echevin, G. Cambon, M. Ramos, O. Astudillo, P. Minnis, and J. K. Ayers (2012), Upwelling response to atmospheric coastal jets off central Chile: A modeling study of the October 2000 event, *J. Geophys. Res.*, *117*, C02030, doi:10.1029/2011JC007446.

Reynolds, R. W., T. M. Smith, C. Liu, D. B. Chelton, K. S. Casey, and M. G. Schlax (2007), Daily high-resolution-blended analyses for sea surface temperature, *J. Clim.*, *20*, 5473–5496.

Rodríguez, E. (2013), ''The Scientific Goals of the RapidScat Mission'', IOVWST (International Ocean Vector Winds Science Team) meeting sponsored by NASA, FSU, COAPS and EUMETSAT, Kona, Hawaii, May 5-8. [Available at http://coaps.fsu.edu/.../Rodriguez_1_RapidScat_OVWST_2013.pdf.]

Small, R. J., S. P. deSzoeke, S. P. Xie, L. O'Neill, H. Seo, Q. Song, P. Cornillon, M. Spall, and S. Minobe (2008), Air-sea interaction over ocean fronts and eddies, *Dyn. Atmos. Oceans*, *45*, 274–319.

Smith, S. D. (1988), Coefficients for sea surface wind stress, heat flux and wind profiles as a function of wind speed and temperature, *J. Geophys. Res.*, *93*, 15,467–15,472.

Song, Q., D. B. Chelton, S. K. Esbensen, N. Thum, and L. W. O'Neil (2009), Coupling between sea-surface temperature and low-level winds in mesoscale numerical models, *J. Clim.*, *22*, 146–164.

Stiles, B. (2014), ''Discovering a decade of coastal winds from scatterometers'', IOVWST (International Ocean Vector Winds Science Team) meeting sponsored by NASA, FSU, COAP, EUMETSAT, CNES, ESA and Ifremer, Brest, France, 2–4 June.

Troupin, C., E. Mason, J. M. Beckers, and P. Sangrà (2012), Generation of the Cape Ghir upwelling filament: A numerical study, *Ocean Model.*, *41*, 1–15.

Wallace, J. M., C. Smith, and Q. Jiang (1990), Spatial patterns of atmosphere-ocean interaction in the Northern Winter, *J. Clim.*, *3*, 990–998.

Wooster, W. S., A. Bakun, and D. R. McLain (1976), The seasonal upwelling cycle along the eastern boundary of the North Atlantic, *J. Mar. Res.*, *34*, 131–141.

Xie, S. P. (2004), Satellite observations of cool ocean-atmosphere interaction, *Bull. Am. Meteorol. Soc.*, *85*, 195–208.